Energy and Buildings 136 (2017) 161–172

Contents lists available at ScienceDirect

Energy and Buildings

journal homepage: www.elsevier.com/locate/enbuild

The impact of evaporation from porous tile on roof thermal performance: A case study of Guangzhou's climatic conditions

Lei Zhang[a,b,*], Rongpeng Zhang[b], Yu Zhang[c,b], Tianzhen Hong[b], Qinglin Meng[a], Yanshan Feng[a]

[a] Building Energy and Environment Laboratory, School of Architecture, Guangzhou Municipal Key Laboratory of Landscape Architecture, State Key Lab of Subtropical Building Science, South China University of Technology, Wushan Road, Tianhe District, Guangzhou 510641, PR China
[b] Building Technology and Urban Systems Division, Lawrence Berkeley National Laboratory, Berkeley, CA 94720, USA
[c] School of Chemistry and Chemical Engineering, South China University of Technology, Wushan Road, Tianhe District, Guangzhou 510641, PR China

ARTICLE INFO

Article history:
Received 31 May 2016
Received in revised form 30 October 2016
Accepted 3 December 2016
Available online 6 December 2016

Keywords:
Passive techniques
Evaporative cooling
Porous building material
Roof thermal performance

ABSTRACT

The evaporative-cooling roof is a popular passive energy conservation technique. This article presents a novel approach for modelling and analysing the influence of evaporation on roof thermal performance. A multivariate nonlinear model was developed for the prediction of the evaporation rate from porous tile. A computer program was then developed based on the one-dimensional roof unsteady heat transfer theory. Finally, the computer program and hourly weather data of Guangzhou, China, were used to analyse the impacts of evaporation (including the evaporation start time and water-application frequency) and slope orientation on roof thermal performance. Evaporation beginning at 11:00 can reduce the external surface temperatures of a horizontal roof and 30°-inclined east-sloping and west-sloping roofs by up to 11.3, 10.7, and 9.8 °C, respectively, from those of a non-evaporative roof. This, in turn, can reduce the peak-hour (16:00–20:00) internal surface heat flux. Additionally, with the horizontal roof, the reduction in the peak-hour heat flux can be doubled if the evaporative layer is frequently replenished with water.

1. Introduction

Guangzhou, one of the largest cities in southern China, is located about 120 km north-northwest of Hong Kong and 145 km north of Macau in a typical subtropical region (23.33°N, 113.5°E). Owing to the hot-humidity climate [1,2] and rapid improvement of living standards [3], the amount of space-cooling equipment in use has increased dramatically over the last 10 years. At the end of 2014, the number of air conditioners owned per 100 households in Guangzhou was 220 units [3], almost three times the national average [4]. The large number of buildings (building area of more than 440 million m^2 at the end of 2014 [3]) and high use of air conditioners during the long summer season have led to high and continuously rising electricity consumption by the building sector of Guangzhou, which will, in turn, have a negative impact on the local environment (in terms of SO_x and NO_x emissions) and global (in terms of CO_2 emission) climate.

Therefore, in Guangzhou as well as China, energy conservation in buildings is a key area in electricity conservation and emission reduction efforts. Both active and passive techniques can be employed in reducing the energy demand of buildings. Measures that use the intrinsic physical mechanisms of a building (e.g. radiation [5], convection [6], heat conduction [7], and phase change [8]) to limit, increase, or convert the energy exchanged between the building and its surrounding environment are passive techniques. In recent years, among the effective strategies addressing climate change and environmental pollution, passive techniques have increasingly attracted the attention of researchers [9].

Evaporative cooling of porous building materials is a passive energy conservation technique. After a porous building material absorbs water, under the combined effects of meteorological factors (including solar radiation, air temperature, humidity, and wind speed) and driven by capillary force, the liquid water in the porous material will gradually move to the material's surface. There, it will convert sensible heat to latent heat in the form of water vapor, which is released into the outdoor environment, thereby reducing the material's surface temperature and the heat flow into the indoor environment, producing a cooling effect [9,10]. The effectiveness

* Corresponding author at: Building Energy and Environment Laboratory, School of Architecture, Guangzhou Municipal Key Laboratory of Landscape Architecture, State Key Lab of Subtropical Building Science, South China University of Technology, Wushan Road, Tianhe District, Guangzhou 510641, PR China.
E-mail address: arzhang@scut.edu.cn (L. Zhang).

http://dx.doi.org/10.1016/j.enbuild.2016.12.012
0378-7788/

Nomenclature

b_1,b_2,b_3	Constants
c	Specific heat (kJ/kg K)
D	Diffuse solar radiation fluxes (W/m^2)
E	Evaporation rate per unit area (kg/m^2 h)
e_a	Actual vapor pressure (kPa)
e_s	Saturation vapor pressure (kPa)
G	Globle solar radiation fluxes (W/m^2)
h	Solar altitude angle (°)
h_0	External surface combined heat transfer coefficient (W/m^2 K)
h_i	Internal surface combined heat transfer coefficient (W/m^2 K)
I	Direct solar radiation fluxes (W/m^2)
k	Number of layer
m	Number of time
m_a	Air masse (dimensionless)
q_c	Surface combined heat transfer (W/m^2)
q_e	External evaporative latent heat flux (W/m^2)
q_i	Internal surface heat flux (W/m^2)
q_s	External surface net shortwave radiation (W/m^2)
Q_s	Surface heat flux (MJ/m^2)
R_n	Surface net radiation (MJ/m^2)
Rh	Relative humidity (%)
t_a	Hourly air temperature (°C)
t_i	Indoor air temperature (°C)
t_p	Dew point temperature (°C)
$t_{s,e}$	External surface temperature (°C)
$t_{s,i}$	Internal surface temperature (°C)
u	Hourly wind velocity (m/s)
α	Surface solar absorptivity
β	Incidence angle (°)
γ	Psychrometer constant (kPa/°C)
Δ	Slope of saturation vapor pressure curve (kPa/°C)
θ	Roof incline angle (°)
λ	Thermal conductivity (W/m K)
ρ	Density (kg/m^3)
τ	Time (s)
τ_o	Atmospheric transmittance (dimensionless)

of evaporative cooling has been proved in different climatic situations, not only in hot and dry regions where it was initially applied [11–13] but also in hot and humid regions [14–16].

Most previous studies on this topic have investigated evaporative cooling at the material level using measurement data. Wanphen et al., selected four materials (pebbles, silica sand, volcanic ash, and siliceous shale) to study. The authors tested the moisture and thermal performance of these four materials under simple boundary conditions. Then, in a wind tunnel that could simulate solar radiation, temperature, and humidity, the researchers cyclically obtained evaporation, surface temperature, and heat flow data of these four materials. The test results indicate that porous material can effectively reduce the surface temperature, where the degree of reduction in the surface temperature is closely related to the moisture content of the material, absorption coefficient of solar radiation, wind speed, and evaporation [17]. Pires et al., suggested that the water-storage medium is the important factor that affects the evaporative cooling effect. To obtain the ideal water-storage medium required in their subsequent study, the researchers studied the evaporative cooling capacity of six types of building materials and five types of textile fabrics in a small wind tunnel with a fixed wind speed and temperature. The experimental results showed that among the construction materials, the performance of the ceramic hollow brick was the best; among the textile fabrics, the performances of the fabric samples with cavities were the best. The authors eventually determined that polyester fabric with honeycomb cavities should be used as the sample for the following evaporative cooling study [18]. He et al., and Chen et al., constructed a passive evaporative cooling wall (PECW) out of moist void bricks [19], or pipe-shaped porous ceramics [20,21] that were capable of absorbing water and allowed wind penetration, thus reducing their surface temperature via water evaporation. Karamanis et al., optimised the selection and preparation of porous materials using the Kelvin equation and validated the optimisation via solar-heat transformation experiments [22].

To analyse more precisely of the evaporative cooling effect from roof porous layer, a mathematical description for predicting roof hygrothermal dynamics is required [23]. Most existing building hygrothermal models were based on the theory of Philip and De Vries, which is one of the most disseminated and accepted mathematical formulation for studying heat and moisture transfer through building porous media, considering both capillary migration and vapor diffusion [23,24]. However, several constraints such as moisture content strongly dependent properties, high nonlinearities and low time step make the model complex and computationally slow [23], which may make it difficult to quantitatively determine the effects of evaporative cooling products on building envelope thermal performance.

The purpose of this paper is to present a novel approach to the investigation of the influence of evaporation on roof thermal performance. As the present study is focused on the numerical method rather than on heat and mass transfer model itself, a complete discussion about mathematical models was avoided. The article is organised as follows: Section 2 describes methodology and material. As described in Subsection 2.1, a multivariate nonlinear model was developed for the prediction of the evaporation rate from porous tile using experimental data and regression analysis. As described in Subsection 2.2, based on the one-dimensional roof unsteady heat transfer model, a computer program that considered the roof surface evaporation latent heat flux using the multivariate nonlinear model was developed. Subsections 2.3 and 2.4 introduce the specific roof constructions and hourly weather data of Guangzhou. Section 3 presents an analysis of the impacts of evaporation start time, water-replenishing frequency, and slope orientation on the thermal performances of specific roof constructions. The results are also discussed in this section. Finally, the major conclusions are summarised in Section 4.

2. Methodology and material

2.1. Multivariate nonlinear model of evaporation rate

The evaporation rate is one of the key parameters in the evaluation of the evaporative latent heat flux of wet surfaces. Researchers recently successfully introduced the Penman-Monteith (P-M) equation, which was initially applied to calculate soil evaporation rate in Pedology field [25,26], to estimate the evaporation rate from wet porous building materials [16,27].

As shown in Eq. (1) [16], the independent variables in the P-M equation include solar radiation, ambient air temperature, relative humidity, wind velocity, and surface heat flux.

$$E = \frac{b_1 \Delta (R_n - Q_s)}{\Delta + \gamma(1 + b_3 u)} + \frac{b_2 \frac{\gamma}{t_a + 273} u (e_s - e_a)}{\Delta + \gamma(1 + b_3 u)} \quad (1)$$

In simulations of building energy consumption, solar radiation, ambient air temperature, relative humidity, and wind velocity data can be easily accessed from typical meteorological year data, while the surface heat flux is obtained through the calculation of surface

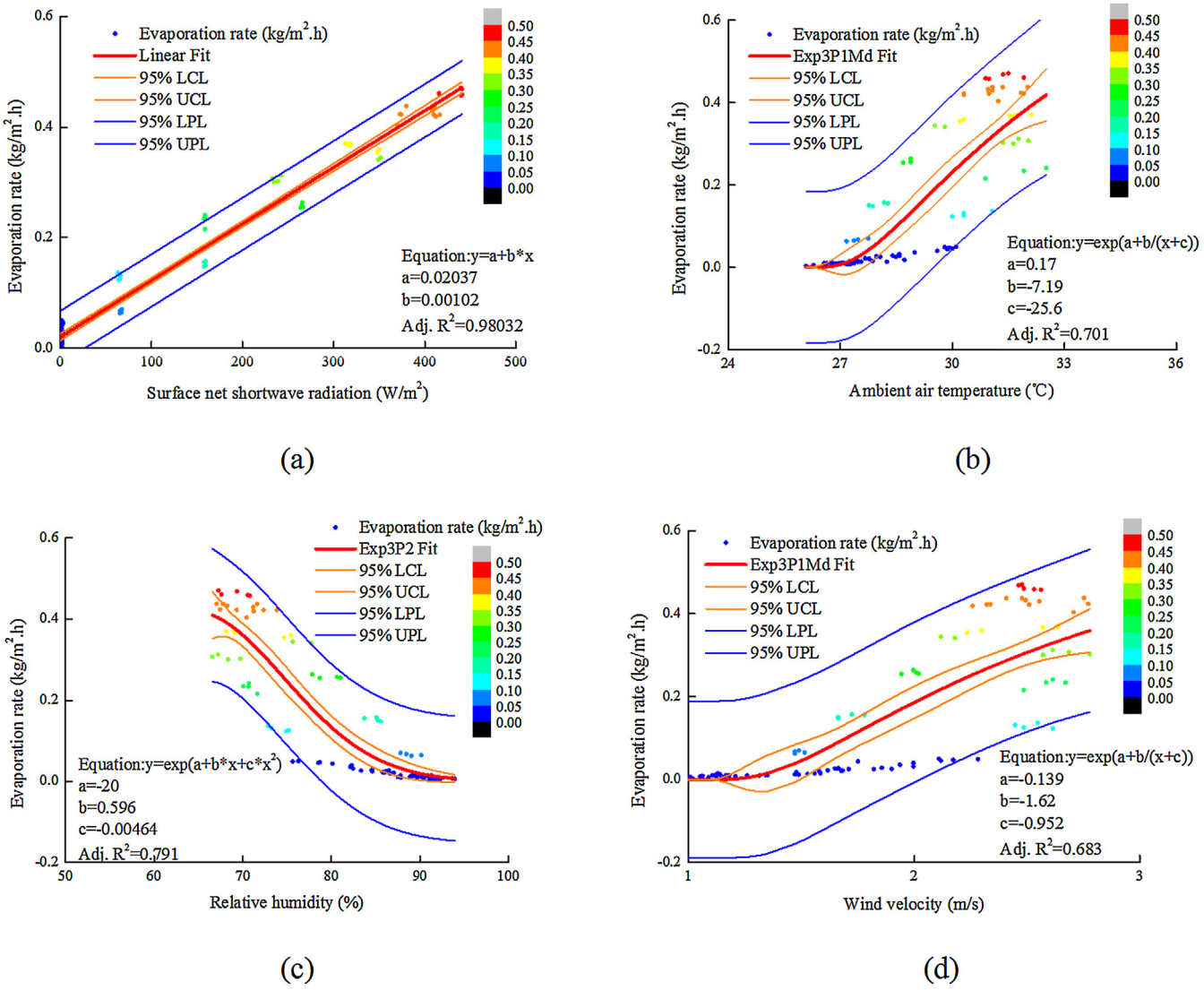

Fig. 1. Relationships between impact factors and evaporation rate.

heat balance and building envelope heat transfer. Additionally, the surface heat flux is coupled with the evaporation process; thus, iterative method is used to obtain the results, which need perform a mathematically rigorous convergence analysis and, this in turn, complicate the calculation. To solve this issue, we employed a simplified model to predict evaporation rate during the building energy simulation process. In our previous study [16], using a climatic wind tunnel, we measured the independent variables of the P-M equation and then determined the hourly evaporation amount. In present work, regression analysis was conducted using the experimental data. Firstly, the unitary regression equations between the four individual independent variables and evaporation rate were established. Secondly, a multivariate nonlinear regression model was proposed based on the four unitary regression equations. Finally, OriginPro software was used for regression of the coefficients in the model.

The unitary regression equations between the four individual independent variables and the evaporation rate are shown in Fig. 1. A significant linear relationship ($R^2 = 0.9803$) between the evaporation rate and surface net shortwave radiation was observed, as shown in Fig. 1(a). The linear regression equation predicted the evaporation rate to be constant at 0.02 kg/m^2·h when the surface net shortwave radiation is 0 W/m^2. According to the P-M equation, when the surface net shortwave radiation is 0 W/m^2, the evaporation rate varies with the partial pressure difference in water vapor between the wet surface and ambient air. Thus, three other independent variables should be considered in addition to the surface net shortwave radiation: ambient air temperature, relative humidity, and wind velocity. As shown in Fig. 1(b-d), we introduced exponential functions to describe the nonlinear regression equations for the three individual independent variables.

To model the comprehensive influence of the radiation and the aerodynamic terms, we developed a multivariate nonlinear regression model, as shown in Eq. (2):

$$E = a_1 \cdot x_1 + e^{\left(a_2 + \frac{a_3}{x_2 + a_4}\right)} + e^{\left(a_5 + a_6 \cdot x_3 + a_7 \cdot x_3^2\right)} + e^{\left(a_8 + \frac{a_9}{x_4 + a_{10}}\right)} + a_{11} \quad (2)$$

where a_1-a_{11} are regression model coefficients, and x_1-$x_4$are the surface net shortwave radiation, ambient air temperature, relative humidity, and wind velocity, respectively.

The values of a_1-a_{11} were obtained via regression analysis using OriginPro, and the statistical model for calculation of the evaporation rate is shown in Eq. (3), as follows:

$$E = 0.000842 \cdot q_s + e^{1.45 - \frac{77.2}{t_a - 14.4}} + e^{1.3 \cdot R_h - 0.01 \cdot R_h^2 - 45.6} + e^{-1.2 - \frac{7.24}{u + 0.355}} - 0.00399 \quad (3)$$

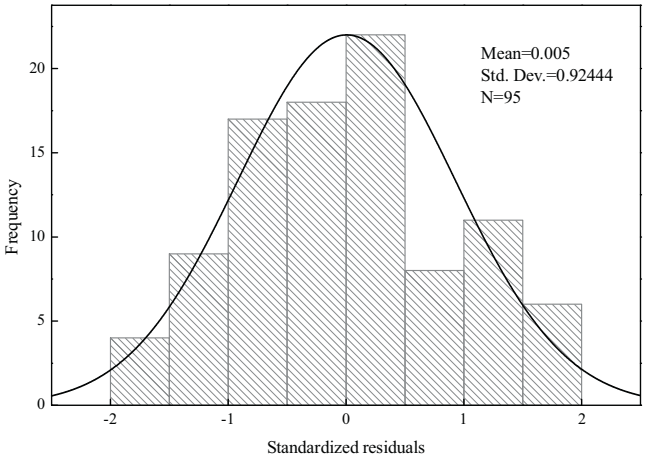

Fig. 2. Histogram of standardised residuals.

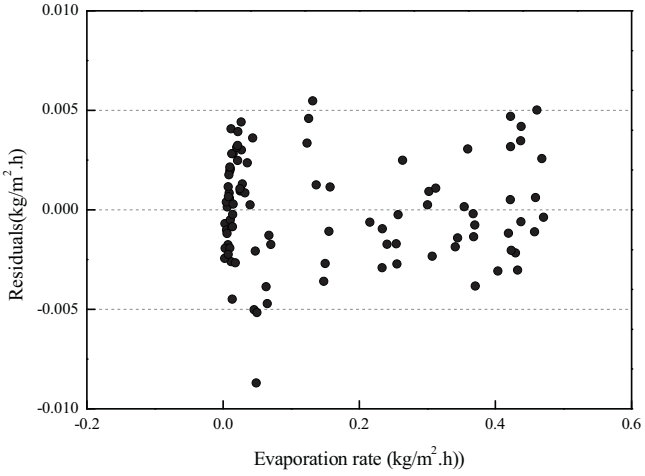

Fig. 3. Residual distribution of measured and predicted evaporation rates.

The range of variation in the independent variables in Eq. (3) is shown in Table 1.

Although the adjusted R^2 values of the regression equations between the evaporation rate and ambient temperature, relative humidity, and wind velocity were lower than 0.8, the adjusted R^2 of the synthesised regression Eq. (3) was 0.99973. Further, the F-test was highly significant ($F = 60465$, $P < 0.001$), reflecting acceptable correlation coefficients of the synthesised regression equation. In addition, the histogram plotted in Fig. 2 depicts a normal distribution of standardised residuals. Fig. 3 plots the distribution of residuals between the measured and predicted evaporation rates. We observed that (1) the distribution of predicted evaporation rates closely matched that of the measured values, (2) the absolute values of the residuals did not exceed 0.009 kg/m^2 h, and (3) the residuals were nearly constant with different measured evaporation rates, reflecting homoscedasticity.

Based on the aforementioned tests, we can conclude that the statistical model for the evaporation rate obtained via the regression method is statistically significant with practical value and high reliability and therefore can be used to estimate variation in the evaporation rate.

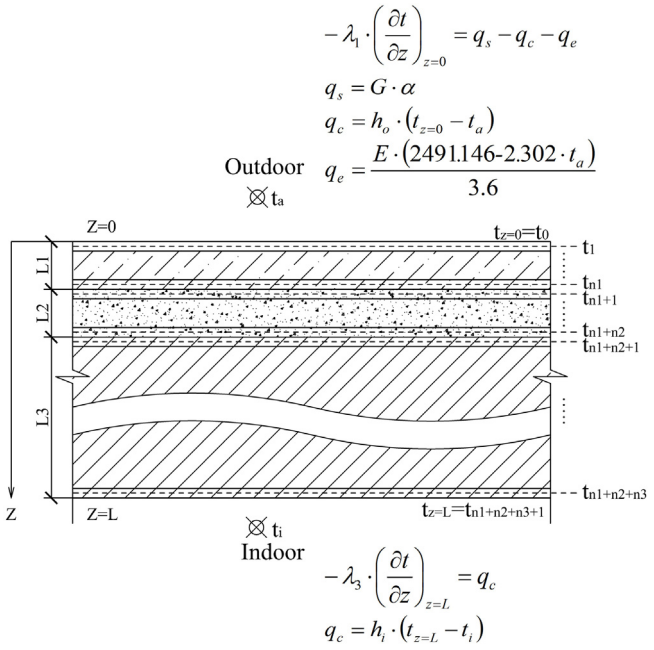

Fig. 4. Schematic representation of the roof.

2.2. One-dimensional unsteady heat transfer of roofs

This subsection presents a procedure for the solution of the unsteady heat flow problem in a composite roof. A schematic representation of the roof is depicted in Fig. 4. The roof's structure comprises three material layers, with thicknesses labelled as L1, L2, and L3.

Based on the physical characteristics of the structures, the problem was solved under the following assumptions: a) internal heat was not generated in any material layer of the roof; b) there was homogeneity in each structure layer, with fixed thermo-physical properties; c) resistance of the layer interface could be ignored, assuming sufficient contact between the material layers; and d) the porous tile layer presented little impact on the conduction process owing to its low thickness; thus, the influence of water content on thermodynamic parameters was ignored.

In accordance with these assumptions, the governing equation and boundary condition were developed. The governing equation is as follows [28,29]:

$$\frac{\partial t}{\partial \tau} = \frac{\lambda}{\rho \cdot c} \cdot \frac{\partial^2 t}{\partial z^2} \quad [0 < z < L] \tag{4}$$

The same equation held true for all three material regions via the insertion of the appropriate λ, ρ, and c values. The condition for the external boundary ($z = 0$), where the roof was exposed to solar radiation, is given by the following equation [16]:

$$-\lambda_1 \cdot \left(\frac{\partial t}{\partial z}\right)_{z=0} = q_s - q_c - q_e \tag{5}$$

where $q_s = G \cdot \alpha$, $q_c = h_o \cdot (t_{z=0} - t_a)$, and $q_e = \frac{E \cdot (2491.146\text{-}2.302 \cdot t_a)}{3.6}$.

In their discussion of the surface heat balance equation, most previous studies have only considered the solar radiation term and the combined convection and radiation heat transfer term [28,29]. In this study, the evaporative latent heat flux, which was calculated using the statistical model in Subsection 2.1, was taken into account.

Table 1
Range of variation in the independent variables.

	Minimum value	Maximum value	Average value	Standard deviation
q_s(W/m^2)	0	440.73	136.09	163.57
t_a(°C)	26.09	32.51	29.04	1.90
R_h(%)	66.59	93.94	81.00	8.96
u(m/s)	0.95	2.78	1.89	0.58

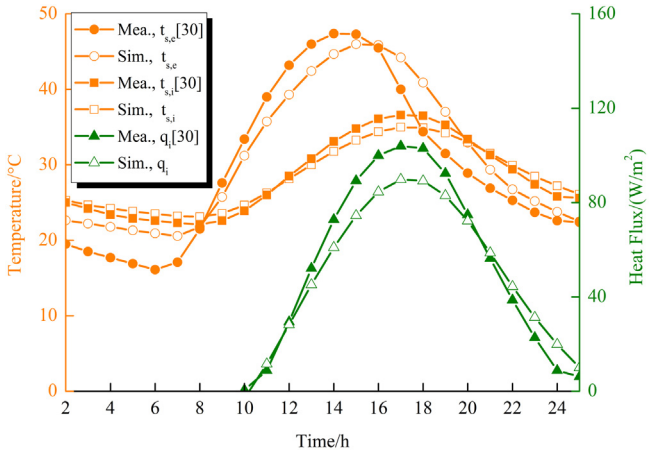

Fig. 5. Variation in heat flux and surface temperature of roof.

In the bottom layer of the concrete slab (z = L), the boundary condition is as follows[28,29]:

$$-\lambda_3 \cdot \left(\frac{\partial t}{\partial z}\right)_{z=L} = q_c \tag{6}$$

where $q_c = h_i \cdot (t_{z=L} - t_i)$. The instantaneous continuity of heat flux and temperature at the interfaces z = L1 and L2 is preserved.

A detailed description of the difference scheme of the derivatives $\frac{\partial t}{\partial \tau}$, $\frac{\partial t}{\partial z}$, and $\frac{\partial^2 t}{\partial z^2}$ is provided in Appendix A.

The governing and boundary conditions were discretised using implicit control volume formulation. An hourly time-step was used within the simulation. The system of equations was solved using the tridiagonal matrix algorithm (TDMA). The initial temperature values were obtained by continuously running the program for several days until the routine daily variation reached a constant calue.

Based on the aforementioned numerical model, a computer program was developed in Visual Basic for roof thermal performance analysis. The program was validated against a case study derived from the previously published work of Kaşka and Yumrutaş [30], who conducted on-site measurements of a concrete roof with 2 cm of plaster on its inside surface and a thickness of 12 cm. The thermophysical properties of the roof's materials are listed in Table 2. The inside air temperature and roof surface solar absorptivity were 25 °C and 0.8, respectively [30]. The combined heat transfer coefficients at the internal and external surfaces were 9 and 22 W/m^2 K, respectively [30].

Fig. 5 shows the daily variation in measured and calculated surface temperatures and heat flow through the roof's structure. The simulated results matched the measured values from the literature well. The mean relative error between the calculated and measured surface temperature was 11.3% for the external surface and 3.2% for the internal surface. The validated computer program was then used to carry out thermal performance analysis of evaporative cooling in the roof.

2.3. Roof with porous material for evaporative cooling

The effectiveness of passive technologies is related to the U-value of building envelopes. Some studies have found that passive technologies like green roofs exert significant cooling effects on un-insulated or moderately insulated buildings owing to the magnitude of ingoing heat fluxes [31]. Thus, in this study, a roof construction without an insulating layer was selected as the research subject for the investigation of the evaporative cooling potential. Specifically, the roof was composed of porous facing tile, cement mortar, and concrete. The porous facing tile was 240 mm long × 50 mm wide × 10 mm thick, and its surface solar absorptivity was 0.76 [15].

Moisture migrating through the building envelope may significantly influence indoor air humidity and air-conditioning loads, especially the latent cooling load [32–36]. To reduce the negative influence of moisture migration, we set up a waterproof film between the porous facing tile and cement mortar. The porous tile layer of the roof product was 10 mm thick, relatively thin compared with the 180-mm concrete layer. Moreover, the waterproof film was impermeable to moisture. Because of the specific roof construction, the moisture transfer between the cement mortar and concrete layer could be negligible, while the facing layer exerted significant influence on the thermal performance of the roof via evaporation.

In our previous study, we measured the mass moisture content variation in the porous facing tile with respect to the soaking time [15]. According to the measurements, after one hour of soaking in water, the mass moisture content of the tile was 7.49%.

The evaporation process in the porous facing tile can be divided into three stages: a constant-rate stage, a falling-rate stage, and a low-rate stage. For the first stage, the evaporation rate is determined by the available energy (radiation) and atmospheric conditions (vapor pressure, wind velocity, etc.). During the second and third stages, the evaporation rate is jointly controlled by the water content, energy supply, and atmospheric conditions. The evaporation rate in the first stage is much higher than that in the second and third stages. Therefore, at the transition between the first and second stages, we determined the critical mass moisture content, below which we ignored the evaporation process, to be 3.1% [15].

The thermal resistance of each material layer, calculated according to the thermodynamic parameters of the material, is shown in Table 3. The combined heat transfer coefficients at the external and internal surfaces were assumed to be 22 and 9 W/m^2 K [30], respectively.

2.4. Generation of hourly weather data

The availability of weather data on small time scales, such as the hourly scale, is vital in the analysis of roof thermal performance. In this study, we used the following methods to generate the hourly weather data of Guangzhou.

2.4.1. Air temperature

The following cosine function was employed for the generation of hourly ambient temperature (t_a) distributions from daily

Table 2
Thermophysical properties of roof materials [30].

Materials	Thermal conductivity (W/m K)	Density (kg/m^3)	Specific heat (J/kg K)
Plaster	0.700	2778	840
Concrete	1.730	2400	840

Table 3
Thermal resistance of each material layer [37].

Description (from outside to inside)	Thickness d (mm)	Thermal conductivity λ (W/m K)	Density ρ (kg/m^3)	Specific heat c (kJ/kg K)	Thermal resistance R = d/λ (m^2 K/W)
Porous facing tile	10	0.24	1654	0.43	0.042
Cement mortar	10	0.93	1800	1.05	0.011
Concrete	180	1.28	2100	0.92	0.141

Note: The waterproof film was very thin; thus, its thermal resistance was ignored.

maximum (t_{max}), minimum (t_{min}), and average (t_{av}) ambient temperatures [38].

$$t_a = \left(\frac{t_{max} - t_{min}}{2}\right) \times \cos\left(\frac{\pi(\tau - 15)}{12}\right) + t_{av} \quad (7)$$

2.4.2. Relative humidity

The hourly relative humidity can be expressed by the following equations [38]:

$$Rh = \exp\left(\frac{17.27 t_p}{t_p + 237.3} - \frac{17.27 t_a}{t_a + 237.3}\right) \quad (8)$$

$$t_p = 0.9153 \times t_{min} + 0.2021 + 0.5 \times \sin\left[(\tau + 1) \times \frac{\pi}{6} - \frac{3 \times \pi}{4}\right] \quad (9)$$

2.4.3. Wind velocity

We assumed that the hourly wind velocity (u) fluctuated randomly between the daily maximum (u_{max}) and minimum (u_{min}) wind speeds. Thus, the hourly wind velocity was computed using the following equation [38]:

$$u = \mathrm{rnd}(0, 1) \times (u_{max} - u_{min}) + u_{min} \quad (10)$$

2.4.4. Solar radiation

The direct (I), diffuse (D), and global solar radiation fluxes (G, the direct plus diffuse radiation; radiation reflected by the ground was assumed to be null for the roof plane) on the roof surface are given by the following formulas [39]:

$$I = I_{SC} \cdot \tau_o^{m_a} \cdot \sin(\beta) \quad (11)$$

$$D = \frac{1}{2} I_{SC} \sin \quad h \frac{1 - \tau_o^{m_a}}{1 - 1.4 \ln \tau_o} \cos^2 \frac{\theta}{2} \quad (12)$$

As shown in Fig. 6, the hourly weather data for 21 July in Guangzhou, obtained using Eqs. (7–12), were used for the following roof thermal performance calculation. The indoor air temperature was set to a constant value of 26 °C. Other boundary conditions, including the surface solar absorptivity, thermal resistance of each layer, and combined heat transfer coefficients at the external and internal surfaces, are listed in Subsection 2.3.

3. Results and discussion

Using the computer program and weather data described in Section 2, the influence of the evaporation start time and water-application frequency on roof thermal performance was analysed, as these two factors considerably affected the evaporation process. Additionally, the impact of roof slope orientation on thermal performance was analysed because it influenced the solar radiation flux on the roof's surface.

The analysis was limited to the calculation of the external surface temperature and the internal surface heat flux of the roof because these factors exert significant influence on the outdoor thermal environment and indoor cooling load.

3.1. Evaporation start time

As noted in Subsection 2.1, the evaporation rate is affected significantly by the intensity of solar radiation, which varies throughout the day. Therefore, different evaporation start times can result in varying evaporative latent heat flux and thus differing thermal performance. To analyse the effect of evaporation start time on roof thermal performance, we calculated variation trends in the external surface temperature and the internal surface heat flux of the roof with evaporation beginning at 7:00, 11:00, and 15:00, as shown in Fig. 7.

The cooling impact of evaporation on roof performance was generally found to last for 2–5 h. In the example case of the evaporation start time of 7:00, after water application, the mass moisture content of the evaporative layer is 7.49%, as shown in Fig. 7(a). Subsequently, evaporation begins, and the mass moisture content of the evaporative layer gradually decreases. At 10:00, the mass moisture content of the evaporative layer drops to 3.3%, close to the critical mass moisture content of 3.1%. Afterwards, the evaporation process is relatively weak and can be ignored. Fig. 7(b) shows the variation in evaporation rate corresponding to the mass moisture content variation in Fig. 7(a). After evaporation begins at 7:00, the evaporation rate continues to increase with gradually increasing solar radiation intensity. From 9:01 to 10:00, the evaporation rate peaks in this case at 0.32 kg/m^2 h. After 11:00, the mass moisture content of the evaporative layer is equal to the critical mass moisture content; therefore, the evaporation rate is zero. The variation in the evaporation rate directly affects the evaporative latent heat flux and thus the roof's external surface temperature. As shown in Fig. 7(c), the external surface temperature of the roof with evaporative cooling equals that without evaporative cooling. Once the evaporation process begins, it consumes a portion of the incident solar radiation, resulting in a slower increase in surface temperature. At 10:00, when the evaporation rate peaks, 52.0% of the incidental solar radiation heat is consumed by evaporation, causing the external surface temperature of the evaporative-cooling roof to be 9.0 °C lower than that of the non-evaporative roof. At 12:00, because the mass moisture content of the evaporative layer reaches its critical point, evaporation weakens, and the effect of evaporative cooling is suppressed. Consequently, the external surface temperature significantly increases, nearing that of the non-evaporative roof and signalling the end of the evaporative cooling effect. Fig. 7(d) shows the variation in the internal surface heat flux. After evaporation begins, the flux of the evaporative-cooling

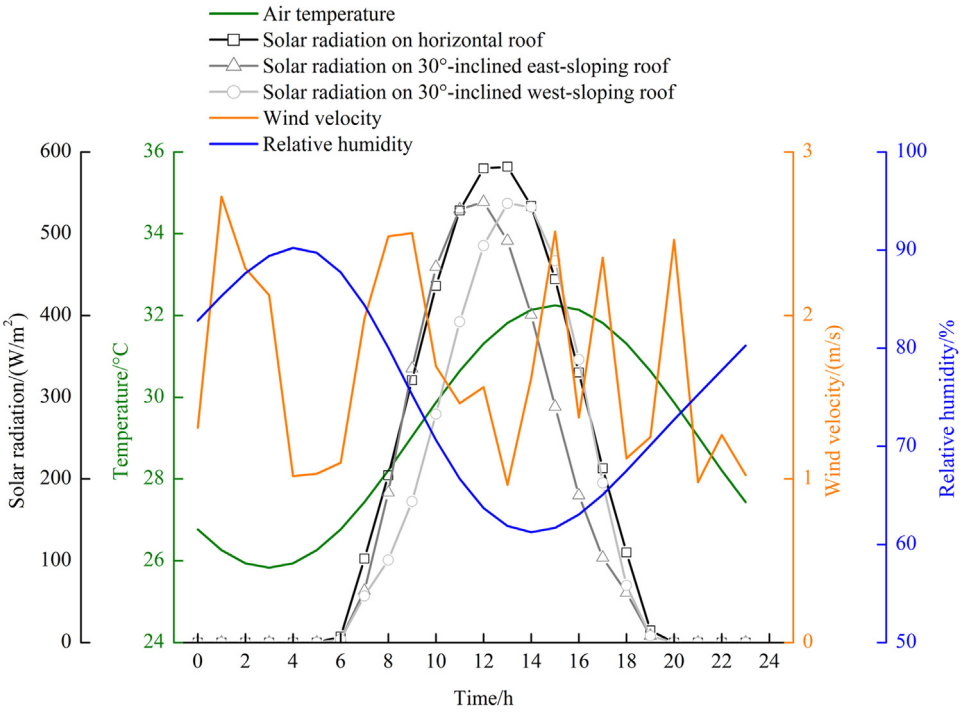

Fig. 6. Hourly weather data on 21 July in Guangzhou.

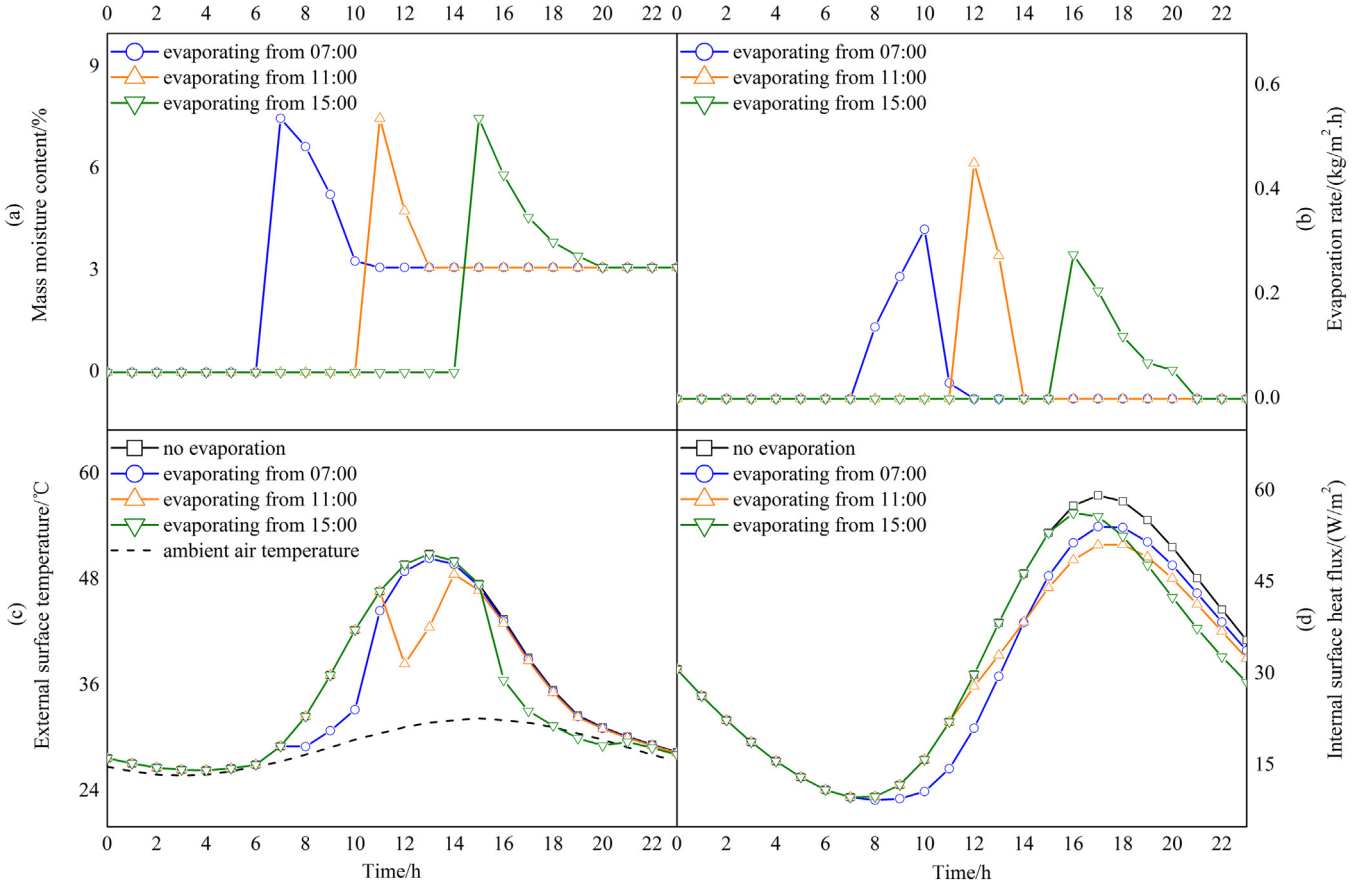

Fig. 7. Impact of evaporation start time on roof thermal performance.

Table 4
Average decrease in external surface temperature and cumulative decrease in internal surface heat flux.

Evaporation start time	Average decrease in external surface temperature (°C)			Cumulative decrease in internal surface heat flux (W/m^2)		
	6:00–11:00	12:00–18:00	19:00–23:00	6:00–11:00	12:00–18:00	19:00–23:00
07:00	3.5	0.3	0.1	15.7	48.2	12.8
11:00	0.0	3.3	0.1	0.0	48.3	22.0
15:00	0.0	2.4	1.2	0.0	10.3	38.5

roof is lower than that of the non-evaporative roof. At 12:00, the difference in the internal surface heat flux between the evaporative cooling and non-evaporative roofs is greatest at 8.8 W/m^2. The heat flux reduction persists owing to the time-lag effect of the building envelope. At 17:00, the internal surface heat flux of the evaporative-cooling roof peaks at 54.2 W/m^2.

With the evaporation start times of 11:00 and 15:00, variations in the external surface temperature and internal surface heat flux of the evaporative roof are similar to those with the start time of 7:00. However, because solar radiation levels differ between these times, the evaporation rate profiles also differ, which further affects the external surface temperature profile and the decrease in the internal surface heat flux. Detailed comparisons are shown in Table 4.

In the daytime (6:00–18:00), solar radiation is intense, and cooling caused by evaporation is significant. Thus, the average decrease in the external surface temperature of the evaporative-cooling roof in the daytime is higher than that at night (19:00–23:00). Consider the case of the evaporation start time of 11:00 as an example: Because no evaporation occurs before 11:00, the average decrease in the external surface temperature is 0 °C. From 12:00 to 18:00, owing to intense solar radiation, cooling caused by evaporation is significant, and the average decrease in the external surface temperature is 3.3 °C. In contrast, from 19:00 to 23:00, the external surface temperature of the evaporative-cooling roof is only 0.1 °C lower than that of the non-evaporative roof.

In addition, in the case of the evaporation start time of 7:00, the average external surface temperature from 6:00 to 11:00 significantly decreases by 3.5 °C. Because the evaporation rate at 12:00 is close to zero in this case, the surface temperature significantly increases during the high-temperature period from 12:00 to 18:00. Although still lower than the external surface temperature of the non-evaporative roof, the surface temperature decreases by an average of only 0.3 °C. In the case of the evaporation start time of 15:00, the initial external surface temperatures of the evaporative roof equal those of the non-evaporative roof. After evaporation begins, the average decrease in the external surface temperature from 12:00 to 18:00 is significant at 2.4 °C.

Evaporation that begins when solar radiation is intense can consume most of the radiation, reducing the internal surface heat flux. According to the calculations in this study, evaporation beginning at 11:00 can reduce the internal surface heat flux by 35.3 W/m^2 (12.5%) from that of the non-evaporative roof between 16:00 and 20:00, the peak load period for residential buildings [40]. This, in turn, can significantly reduce the heat flux from the roof to the indoor environment and subsequently decrease the energy consumption of air conditioners.

3.2. Water-application frequencies

When the mass moisture content of the evaporative layer reaches its critical point, evaporation is suppressed. Thus, the evaporative layer must be replenished with water for evaporation to continue to cool the roof. In this study, we compared the effects of two water-application conditions with the same evaporation start time (11:00) on the external surface temperature and internal surface heat flux. The first involved one water application (i.e. after evaporation starts at 11:00, there is no further water application), while the second involved multiple instances of water application (i.e. when the mass moisture content of the evaporative layer reaches the critical mass moisture content, water is replenished). The calculation results are shown in Fig. 8.

As shown in Fig. 8(a), the external surface temperature variation after the first application of water in the multiple-application case is similar to that of one water application. After the mass moisture content of the evaporative layer reaches critical mass moisture content at 13:00, water is applicated for the second time between 13:01 and 14:00. Evaporation resumes at 14:00. In the evaporation process over the next 3 h, the surface temperature remains significantly lower than those of the non-evaporative roof and one-time water-application roof. After the third water application between 17:01 and 18:00, evaporation resumes again.

Fig. 8(b) shows that the internal surface heat flux in the case of multiple water applications is significantly lower than that of the non-evaporative roof and one-time water-application roof. At 16:00, the internal surface heat flux in the case of multiple water applications reaches its maximum value, 44.0 W/m^2, 7.2 W/m^2 less than the maximum value with one water application.

Fig. 8(c) and (d) depict the mass moisture content and corresponding evaporation rate profiles of the evaporative layer in the cases of one and multiple water applications. With one water application, when the mass moisture content of the evaporative layer reaches its critical point, evaporation is assumed to cease, and the evaporation rate is therefore zero. In the case of multiple water applications, when the mass moisture content reaches its critical point, water replenishment begins, and the mass moisture content of the evaporative layer increases back to its initial level. Evaporation then resumes, and the mass moisture content of the evaporative layer gradually decreases. When the mass moisture content reaches its critical point again, this whole process repeats.

The average decreases in the external roof surface temperature and the cumulative heat flux of the inner surface for these two water application conditions are shown in Table 5. Because of continuously cooling evaporation, the average decrease in the external surface temperature with multiple water applications is 1.9 times that with one water application between 12:00 and 18:00, whereas the decrease in the cumulative internal surface heat flux is 2 times that with one water application from 16:00 to 20:00.

3.3. Roof slope orientation

Because of the influences of incline angle and slope orientation, solar radiation on an inclined roof differs from that on a horizontal roof, which may affect roof thermal performance calculation results.

Thus, the influence of roof incline angle and slope orientation on thermal performance were analysed in this study. Firstly, the solar radiation levels on three kinds of roofs (one horizontal roof and two inclined roofs, both with a 30° incline but different slope orientations) were calculated. The roofs' external surface temperatures with and without evaporation were then compared for determination of the influence of roof slope orientation on the evaporative cooling effect. The results are shown in Fig. 9.

As shown in Fig. 6 in Subsection 2.4, the greatest solar radiation levels on the horizontal roof and roof sloping west occurred at 13:00

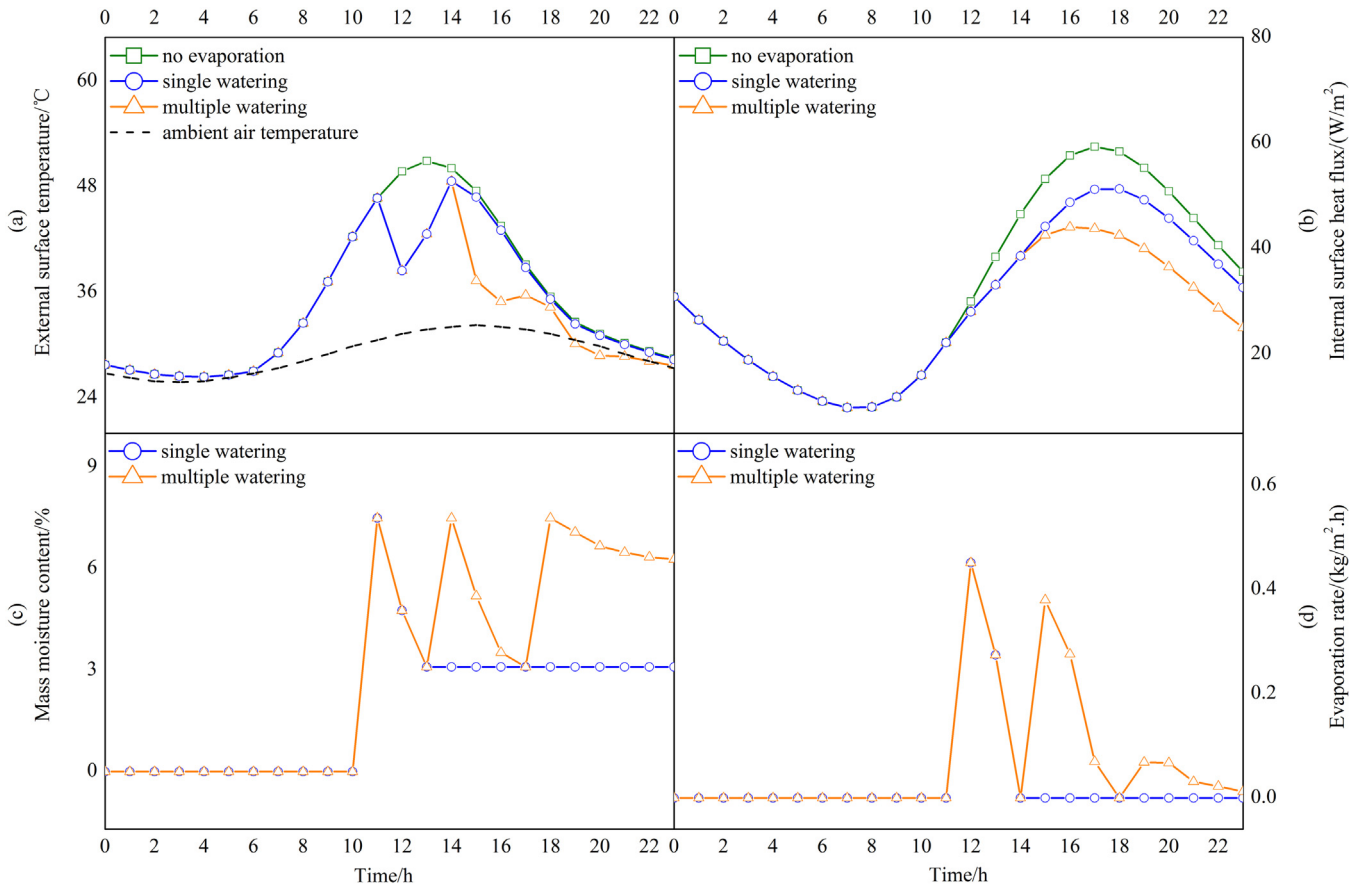

Fig. 8. Impact of water-application frequency on roof thermal performance.

Table 5
Average decrease in external surface temperature and cumulative decrease in internal surface heat flux.

water application conditions	Average decrease in external surface temperature (°C)			Cumulative decrease in internal surface heat flux (W/m²)		
	6:00–11:00	12:00–18:00	19:00–23:00	6:00–11:00	12:00–18:00	19:00–23:00
Single application	0.0	3.3	0.1	0.0	48.3	22.0
Multiple application	0.0	6.4	1.7	0.0	70.8	65.2

at 580 and 537W/m^2, respectively. On the roof sloping east, peak solar radiation occurred at 12:00 at 539 W/m^2.

The maximum external surface temperatures and the times at which they occurred varied with changes in solar radiation, as shown in Fig. 9(a). At 13:00, the external surface temperature of the horizontal roof peaked at 51.1 °C. On the roofs sloping east and west, the external surface temperature peaked at 12:00 and 14:00 at 49.0 and 49.9 °C, respectively.

For the internal surface heat flux, peak and valley values occurred later than those of the external surface temperature owing to the roofs' heat storage performance, as shown in Fig. 9(b). The maximum internal surface heat fluxes on the horizontal, east-sloping, and west-sloping roofs occurred 4–5 h after external surface temperatures peaked and were 59.3, 53.5, and 55.5 W/m^2, respectively.

To illustrate the influence of roof slope orientation on the evaporative cooling effect, we calculated the thermal performance of the three kinds of roofs with the same evaporation start time (11:00) and water application frequency (once). As shown in Fig. 9(c) and (d), when evaporation begins at 11:00, the maximum external surface temperatures of the horizontal, east-sloping, and west-sloping roofs decrease by 2.3, 1.6, and 1.6 °C, respectively, from those of the non-evaporative roof. Further, the maximum internal surface heat fluxes of the horizontal, east-sloping, and west-sloping roofs decrease by 8.0, 8.1, and 7.2 W/m^2, respectively. Although the maximum surface temperature and heat flux values are not significantly different from those of the non-evaporative roofs, the reductions in the average external surface temperature during the evaporation process (12:00-13:00) and in the accumulated internal surface heat flux after evaporation (12:00-23:00) are remarkable, at 9.7–9.8 °C and 12.3% to 13.3%, respectively.

4. Conclusions

In this study, the effect of the evaporation process of porous tile on roof thermal performance was investigated using a novel approach that took into consideration the latent heat flux of evaporation in the roof surface heat balance equation. The main conclusions can be summarised as follows:

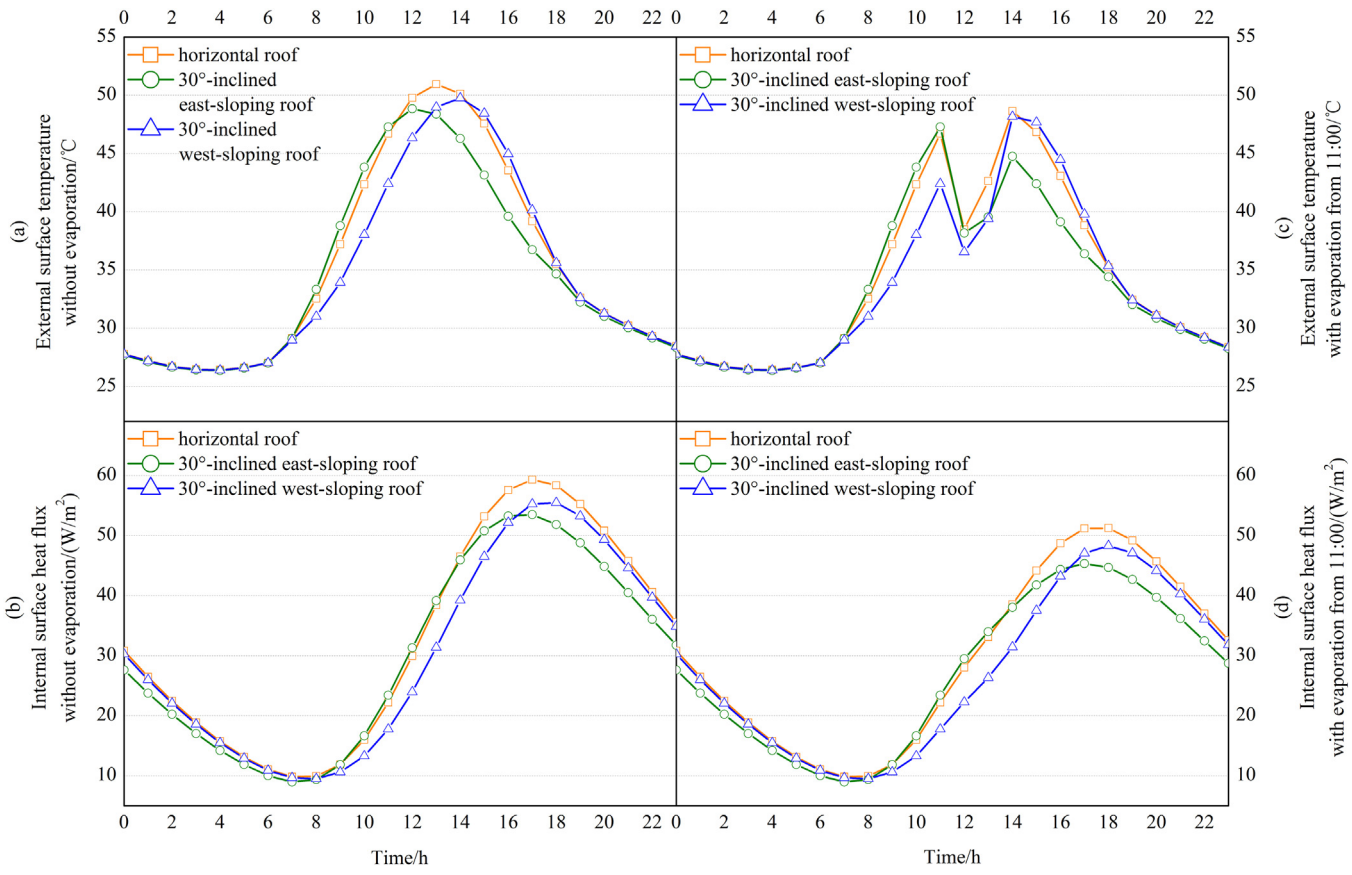

Fig. 9. Impact of roof slope orientation on thermal performance.

(1) A statistically significant positive linear correlation could be observed between the surface net shortwave radiation and evaporation rate (adj. $R^2 = 0.980$), indicating that the evaporation rate and the consequent cooling effect increased with the rise of solar radiation and surface solar absorptance. However, without evaporation on the roof's surface, greater solar absorptance could result in higher surface temperatures. Thus, the coupled influence of surface solar absorptance and the evaporative cooling effect on roof thermal performance should be taken into consideration in future work.

(2) The mass moisture content of the porous tile has remarkable influence on roof thermal performance. When the porous tile contains sufficient water, the evaporation rate and corresponding cooling effect will be much greater, which can decrease the surface temperature by up to 11.3 °C. When the mass moisture content nears or reaches the critical mass moisture content, the evaporation rate decreases significantly, resulting in a weak cooling effect. Future work should also include an analysis of the effects of different water absorptance characteristics of porous tiles and water supply methods on the evaporative cooling effect.

This study focused on the Guangzhou region, which lies in a subtropical climate, and the cooling period. Further studies will certainly be needed to assess the accuracy of the evaporation rate prediction model using other meteorological parameters. Additionally, cases studies with various climatic conditions should be undertaken in the future.

Acknowledgements

This research work was funded by the National Natural Science Foundation of China (No. 51308223, 51678243), Guangdong Natural Science Foundation (No. 2016A030313506) and State Key Lab of Subtropical Building Science, South China University of Technology (No. 2015ZC14).

Appendix A.

The derivatives $\frac{\partial t}{\partial \tau}$, $\frac{\partial t}{\partial z}$, and $\frac{\partial^2 t}{\partial z^2}$, as shown in Eqs. (4–6), were approximated by the following difference schemes, respectively:

$$\frac{\partial t_k}{\partial z} \approx \frac{t_k^m - t_{k-1}^m}{(\Delta z_{k-1} + \Delta z_k)/2} \tag{1a}$$

$$\frac{\partial t_{k+1}}{\partial z} \approx \frac{t_{k+1}^m - t_k^m}{(\Delta z_k + \Delta z_{k+1})/2} \tag{2a}$$

$$\frac{\partial^2 t_k}{\partial z^2} = \frac{\partial\left(\partial t_k/\partial z\right)}{\partial z} \approx \left[\frac{t_{k+1}^m - t_k^m}{(\Delta z_{k+1} + \Delta z_k)/2} - \frac{t_k^m - t_{k-1}^m}{(\Delta z_k + \Delta z_{k-1})/2}\right] / \Delta z_k \tag{3a}$$

$$\frac{\partial t_k}{\partial \tau} \approx \frac{t_k^m - t_k^{m-1}}{\Delta \tau} \tag{4a}$$

The equation for the top volume cell is rewritten below.

$$\left(1 + \frac{\lambda_1}{\Delta z_1 \cdot h_o}\right) t_0^m + \left(-\frac{\lambda_1}{\Delta z_1 \cdot h_o}\right) t_1^m = t_{sol-air}^m \tag{5a}$$

$$t^m_{sol-air} = t^m_a + \frac{q_s(m)}{h_o} - \frac{q_e(m)}{h_o} \tag{6a}$$

In our model, the boundary conditions are limited to the Fourier type in linear form. Consequently, the sol-air temperature approach was used to describe the equivalent outdoor air temperature. However, past studies only took into account the first two items on the right side of Eq. (6a) [28,29], which may overestimate the sol-air temperature with evaporation on the exterior roof surface. Thus, in this study, the sol-air temperature variation due to evaporation was considered as the third item in Eq. (6a).

The equation for the bottom volume cell was rewritten as follows:

$$\left(-\frac{\lambda_3}{\Delta z_3 \cdot h_i}\right) t^m_{n1+n2+n3} + \left(1 + \frac{\lambda_3}{\Delta z_3 \cdot h_i}\right) t^m_{n1+n2+n3+1} = t^m_i \tag{7a}$$

The equation for any volume cell located between the top and bottom volume cells of a particular material was rewritten as follows:

$$(-\gamma_D)\, t^m_{k-1} + (1+2\gamma_D)\, t^m_k + (-\gamma_D)\, t^m_{k+1} = t^{m-1}_k \tag{8a}$$

$$\gamma_D = \frac{\lambda_D \cdot \Delta\tau}{c_D \cdot \rho_D \cdot \Delta z_D^2} \tag{9a}$$

The aforementioned discretised equations were not applicable to volume cells n1, n1 + 1, n1 + n2, and n1 + n2 + 1 because these cells were interface nodes of two different layers.

The equation for volume cell n1 was rewritten as follows:

$$(-\gamma_1) \cdot t^m_{k-1} + \left(1 + \gamma_1 + \gamma_{1,2}\right) \cdot t^m_k + \left(-\gamma_{1,2}\right) \cdot t^m_{k+1} = t^{m-1}_k \tag{10a}$$

where, $\gamma_1 = \frac{\lambda_1 \cdot \Delta\tau}{c_1 \cdot \rho_1 \cdot \Delta z_1^2}$, $\gamma_{1,2} = \frac{2 \cdot \lambda_{1,2} \cdot \Delta\tau}{c_{1,2} \cdot \rho_{1,2} \cdot \Delta z_1 \cdot (\Delta z_1 + \Delta z_2)}$, $\lambda_{1,2} = \frac{\Delta z_1 + \Delta z_2}{\frac{\Delta z_1}{\lambda_1} + \frac{\Delta z_2}{\lambda_2}}$, $\rho_{1,2} = \frac{\rho_1 \cdot \Delta z_1 + \rho_2 \cdot \Delta z_2}{\Delta z_1 + \Delta z_2}$, $c_{1,2} = \frac{c_1 \cdot \Delta z_1 + c_2 \cdot \Delta z_2}{\Delta z_1 + \Delta z_2}$.

The equation for volume cell n1 + 1 was rewritten as follows:

$$\left(-\gamma_{2,1}\right) \cdot t^m_{k-1} + \left(1 + \gamma_{2,1} + \gamma_2\right) \cdot t^m_k + (-\gamma_2) \cdot t^m_{k+1} = t^{m-1}_k \tag{11a}$$

where, $\gamma_2 = \frac{\lambda_2 \cdot \Delta\tau}{c_2 \cdot \rho_2 \cdot \Delta z_2^2}$ and $\gamma_{2,1} = \frac{2 \cdot \lambda_{1,2} \cdot \Delta\tau}{c_{1,2} \cdot \rho_{1,2} \cdot \Delta z_2 \cdot (\Delta z_1 + \Delta z_2)}$.

The equation for volume cell n1 + n2 was rewritten as follows:

$$(-\gamma_2) \cdot t^m_{k-1} + \left(1 + \gamma_2 + \gamma_{2,3}\right) \cdot t^m_k + \left(-\gamma_{2,3}\right) \cdot t^m_{k+1} = t^{m-1}_k \tag{12a}$$

where, $\gamma_{2,3} = \frac{2 \cdot \lambda_{2,3} \cdot \Delta\tau}{c_{2,3} \cdot \rho_{2,3} \cdot \Delta z_2 \cdot (\Delta z_2 + \Delta z_3)}$, $\lambda_{2,3} = \frac{\Delta z_2 + \Delta z_3}{\frac{\Delta z_2}{\lambda_2} + \frac{\Delta z_3}{\lambda_3}}$, $\rho_{2,3} = \frac{\rho_2 \cdot \Delta z_2 + \rho_3 \cdot \Delta z_3}{\Delta z_2 + \Delta z_3}$, $c_{2,3} = \frac{c_2 \cdot \Delta z_2 + c_3 \cdot \Delta z_3}{\Delta z_2 + \Delta z_3}$.

The equation for volume cell n1 + n2 + 1 was rewritten as follows:

$$\left(-\gamma_{3,2}\right) \cdot t^m_{k-1} + \left(1 + \gamma_{3,2} + \gamma_3\right) \cdot t^m_k + (-\gamma_3) \cdot t^m_{k+1} = t^{m-1}_k \tag{13a}$$

where, $\gamma_3 = \frac{\lambda_3 \cdot \Delta\tau}{c_3 \cdot \rho_3 \cdot \Delta z_3^2}$, $\gamma_{3,2} = \frac{2 \cdot \lambda_{2,3} \cdot \Delta\tau}{c_{2,3} \cdot \rho_{2,3} \cdot \Delta z_3 \cdot (\Delta z_2 + \Delta z_3)}$.

References

[1] Z. Han, Q. Liu, Y. Zhang, S. Zhang, J. Liu, W. Li, Feasibility study on novel room air conditioner with natural cooling capability, Appl. Therm. Eng. 108 (2016) 1310–1319.

[2] L. Yang, J.C. Lam, J. Liu, C.L. Tsang, Building energy simulation using multi-years and typical meteorological years in different climates, Energy Convers. Manage. 49 (1) (2008) 113–124.

[3] Statistics Bureau of Guangzhou Municipality, Guangzhou Statistical Yearbook, 2015.

[4] National Bureau of Statistics PRC, China Statistical Yearbook 2015 (Chinese-English Edition), China Statistics Press, 2015.

[5] A.P. Raman, M.A. Anoma, L. Zhu, E. Rephaeli, S. Fan, Passive radiative cooling below ambient air temperature under direct sunlight, Nature 515 (7528) (2014) 540–544.

[6] S. Mirrahimi, M.F. Mohamed, L.C. Haw, N.L.N. Ibrahim, W.F.M. Yusoff, A. Aflaki, The effect of building envelope on the thermal comfort and energy saving for high-rise buildings in hot–humid climate, Renew. Sustain. Energy Rev. 53 (2016) 1508–1519.

[7] L.E. Mavromatidis, M.E. Mankibi, P. Michel, M. Santamouris, Numerical estimation of time lags and decrement factors for wall complexes including Multilayer Thermal Insulation, in two different climatic zones, Appl. Energy 92 (2012) 480–491.

[8] H. Akeiber, P. Nejat, M.Z.A. Majid, M.A. Wahid, F. Jomehzadeh, I.Z. Famileh, et al., A review on phase change material (pcm) for sustainable passive cooling in building envelopes, Renew. Sustain. Energy Rev. 60 (2016) 1470–1497.

[9] S.B. Sadineni, S. Madala, R.F. Boehm, Passive building energy savings: a review of building envelope components, Renew. Sustain. Energy Rev. 15 (8) (2011) 3617–3631.

[10] M. Santamouris, D. Kolokotsa, Passive cooling dissipation techniques for buildings and other structures: the state of the art, Energy Build. 57 (2013) 74–94.

[11] M. Dabaieh, O. Wanas, M.A. Hegazy, E. Johansson, Reducing cooling demands in a hot dry climate: a simulation study for non-insulated passive cool roof thermal performance in residential buildings, Energy Build. 89 (2015) 142–152.

[12] S.N. Kharrufa, Y. Adil, Upgrading the building envelope to reduce cooling loads, Energy Build. 55 (2012) 389–396.

[13] L.C.H. Sosa, G. Gómez-Azpeitia, Cooling average potential of evaporative cooling system in dry warm climate, Energy Proc. 57 (2014) 2554–2563.

[14] W. Yang, Z. Wang, X. Zhao, Experimental investigation of the thermal isolation and evaporative cooling effects of an exposed shallow-water-reserved roof under the sub-tropical climatic condition, Sustain. Cities Soc. 14 (2015) 293–304.

[15] L. Zhang, X. Liu, Q. Meng, Y. Zhang, Experimental study on the impact of mass moisture content on the evaporative cooling effect of porous face brick, Energy Effic. 9 (2) (2016) 511–523.

[16] L. Zhang, Y. Feng, Q. Meng, Y. Zhang, Experimental study on the building evaporative cooling by using the Climatic Wind Tunnel, Energy Build. 104 (2015) 360–368.

[17] S. Wanphen, K. Nagano, Experimental study of the performance of porous materials to moderate the roof surface temperature by its evaporative cooling effect, Build. Environ. 44 (2) (2009) 338–351.

[18] L. Pires, P.D. Silva, J.P. Castro Gomes, Performance of textile and building materials for a particular evaporative cooling purpose, Exp. Therm. Fluid Sci. 35 (4) (2011) 670–675.

[19] J. He, A. Hoyano, A 3D CAD-based simulation tool for prediction and evaluation of the thermal improvement effect of passive cooling walls in the developed urban locations, Sol. Energy 83 (7) (2009) 1064–1075.

[20] J. He, A. Hoyano, Experimental study of cooling effects of a passive evaporative cooling wall constructed of porous ceramics with high water soaking-up ability, Build. Environ. 45 (2) (2010) 461–472.

[21] W. Chen, S. Liu, J. Lin, Analysis on the passive evaporative cooling wall constructed of porous ceramic pipes with water sucking ability, Energy Build. 86 (2015) 541–549.

[22] D. Karamanis, E. Kyritsi, S. Krimpalis, Well-ordered nanoporous materials for low-temperature water phase changes and solar evaporative cooling, Sol. Energy Mater. Sol. Cells 139 (2015) 34–43.

[23] G.H. dos Santos, N. Mendes, Numerical analysis of passive cooling using a porous sandy roof, Appl. Therm. Eng. 51 (1) (2013) 25–31.

[24] N. Mendes, P.C. Philippi, R. Lamberts, A new mathematical method to solve highly coupled equations of heat and mass transfer in porous media, Int. J. Heat Mass Transfer 45 (3) (2002) 509–518.

[25] R. Rivas, V. Caselles, A simplified equation to estimate spatial reference evaporation from remote sensing-based surface temperature and local meteorological data, Remote Sens. Environ. 93 (1) (2004) 68–76.

[26] P. Hughes, N.J. Mason, Introduction to Environmental Physics: Planet Earth, Life and Climate, CRC Press, 2014, pp. 353–354.

[27] M.M. Davis, S. Hirmer, The potential for vertical gardens as evaporative coolers: an adaptation of the 'Penman Monteith Equation', Build. Environ. 92 (2015) 135–141.

[28] K.T. Zingre, M.P. Wan, S.K. Wong, W.B.T. Toh, I.Y.L. Lee, Modelling of cool roof performance for double-skin roofs in tropical climate, Energy 82 (2015) 813–826.

[29] O.A. Zainal, R. Yumrutaş, Validation of periodic solution for computing CLTD (cooling load temperature difference) values for building walls and flat roofs, Energy 82 (2015) 758–768.

[30] Ö. Kaşka, R. Yumrutaş, Comparison of experimental and theoretical results for the transient heat flow through multilayer walls and flat roofs, Energy 33 (12) (2008) 1816–1823.

[31] M. D'Orazio, C. Di Perna, E. Di Giuseppe, Green roof yearly performance: a case study in a highly insulated building under temperate climate, Energy Build. 55 (2012) 439–451.

[32] H.L. Hens, Combined heat, air, moisture modelling: a look back, how, of help? Build. Environ. 91 (2015) 138–151.

[33] M. Van Belleghem, M. Steeman, H. Janssen, A. Janssens, M. De Paepe, Validation of a coupled heat, vapour and liquid moisture transport model for porous materials implemented in CFD, Build. Environ. 81 (2014) 340–353.

[34] G.H. dos Santos, N. Mendes, Heat, air and moisture transfer through hollow porous blocks, Int. J. Heat Mass Transfer 52 (9) (2009) 2390–2398.

[35] K. Abahri, R. Belarbi, A. Trabelsi, Contribution to analytical and numerical study of combined heat and moisture transfers in porous building materials, Build. Environ. 46 (7) (2011) 1354–1360.

[36] M. Qin, R. Belarbi, A. Ait-Mokhtar, L.O. Nilsson, Coupled heat and moisture transfer in multi-layer building materials, Constr. Build. Mater. 23 (2) (2009) 967–975.
[37] People's Republic of China national standard: thermal design code for civil building GB 50176-93, Ministry of Housing and Urban-Rural Development of the People's Republic of China, Beijing, 1993.
[38] B. Debele, R. Srinivasan, J.Y. Parlange, Accuracy evaluation of weather data generation and disaggregation methods at finer timescales, Adv. Water Resour. 30 (5) (2007) 1286–1300.
[39] Handbook, ASHRAE Fundamentals, American society of heating, refrigerating and air-conditioning engineers. Inc., Atlanta, GA, USA, 2009.
[40] W.J.N. Turner, I.S. Walker, J. Roux, Peak load reductions: electric load shifting with mechanical pre-cooling of residential buildings with low thermal mass, Energy 82 (2015) 1057–1067.